Environ. Sci. Technol. **2000**, *34,* 137−142

Kinetics of MSWI Fly Ash Thermal Degradation. 2. Mechanism of Native Carbon Gasification

ELENA COLLINA, MARINA LASAGNI, MASSIMO TETTAMANTI, AND DEMETRIO PITEA*

Dipartimento di Scienze dell'Ambiente e del Territorio (DISAT), Universitá degli Studi di Milano-Bicocca, Piazza della Scienza 1, 20126 Milano, Italy

A generalized kinetic model for fly ash native carbon oxidation is developed. It is shown that the conversion of fly ash native carbon to CO_2 is the result of two simultaneous processes taking place on fly ash surface: the first process (rate constant k_2) is the direct oxygen transfer from a metal oxide site to a vacant carbon active site leading to immediate carbon gasification; the second one is dissociative oxygen chemisorption (k_1) followed by C(O) complex intermediate uncatalyzed gasification (k_3). The model is validated using the kinetic data from model systems and those reported in Part 1 for four different fly ashes. The rate constants, k_1, k_2, and k_3, together with activation and thermodynamic parameters are calculated. For each fly ash, the rate determining step is the complex intermediate oxidation. The nature of the interaction between native carbon and the fly ash surface is the key factor for C and C(O) complex formation and gasification.

Introduction

In Part 1 of this series *(1)*, the native carbon thermal degradation of four Municipal Solid Waste Incinerators, MSWIs, fly ash samples was studied. The samples were selected to be representative of two countries (Denmark: FA1 and FA2a,b; Italy: FA3), three MSWIs (Reno-Nord: FA1; Re-Sud: Fa2a,b; Zama: FA3), and different initial carbon contents (the TOC^0 ranged between 2000 and 8000 ppm). We have demonstrated that the main chemical process is carbon oxidation to CO_2 and that, under our experimental conditions, the carbon for the reactions does not come from organic compounds but originate from MSWI fly ash native carbon. At each temperature in the range 200−600 °C, the experimental total organic carbon, TOC-time data were processed with a sum of two exponentials (deconvolution procedure) i.e., in terms of two pseudo-first-order reactions Ri and Rj (eq 1 in ref *1*). The key experimental information for the formulation of a reaction scheme is the temperature dependence of the preexponential C_i and C_j parameters ($C_i + C_j = TOC^0$); C_i, related to the slower Ri process, decreased, while C_j, related to Rj, increased with increasing temperature.

In this work we propose a reaction mechanism for native carbon thermal degradation based both on the elaboration of Part 1 *(1)* experimental results and the previous one obtained on C−SiO_2 model system *(2)*.

* Corresponding author phone: +39-02-26603253; fax: +39-02-70638129; e-mail: d.pitea@csrsrc.mi.cnr.it.

Background

For carbon gasification, it is reported *(3)* that in the 450−850 °C range there are three reaction regimes: at temperatures between 450 and 550 °C (zone I; activation energy of about 200 kJ mol^{-1}), the overall reaction rate is controlled by the inherent chemical reactivity of the carbon; in the temperature range between 550 and 650 °C (zone II; activation energy of about 90 kJ mol^{-1}), the reaction rate is controlled by both surface chemistry and internal mass transport (pore diffusion); at temperatures between 650 and 850 °C (zone III; activation energy above 10 kJ mol^{-1}), the controlling factor is usually external mass transport.

For fly ash reactions**,** it was suggested *(4)* that external mass transfer limitations are not important under simulated postcombustion conditions**.** In fact, fly ash surface areas are generally quite low (1−10 $m^2\,g^{-1}$), suggesting that a significant pore structure is not present; accordingly, internal mass transfer limitations may also be not important.

Carbon gasification can result from both of the two following processes or their combination. One possible process is the direct impingement of oxygen onto vacant carbon active sites, leading to some immediate carbon gasification *(3)*. The active sites on carbon are believed to be the unsaturated carbon atoms with one or two free sp^2 orbitals located at the edge of graphitic sheets or other structural defects, whereas the carbon atoms inside the basal graphitic plane (saturated carbon atoms) are almost inactive *(3)*. Thus, the reactivity is determined by the availability of carbon active sites in the carbon structure which in turns depends on the structural and topochemical characteristics of carbon such as carbon type, crystallite size, porosity, lattice imperfections, and surface properties *(5)*.

In the second process, elementary reactions describing the mechanism details of the chemical reaction scheme are as follows.

(i) Gaseous Oxygen Adsorption and Surface Diffusion. Molecular oxygen can be dissociatively chemisorbed on carbon active sites (uncatalyzed adsorption) or metallic sites (catalyzed adsorption) *(6)*. The hypothesized equations for the dissociative chemisorption of O_2 are

$$C + {}^1/_2O_2 \rightarrow C(O) \quad (1)$$

$$Me + {}^1/_2O_2 \rightarrow MeO \quad (2a)$$

where C is a free site in carbon structure; C(O) a surface complex; Me a metallic site, and MeO the metal oxide. After step 2a, the adsorbed oxygen can migrate from a metallic site to a carbon site:

$$MeO + C \rightarrow Me + C(O) \quad (2b)$$

During the course of low-temperature carbon gasification, a considerable amount of oxygen complexes can build up on the carbon surface. It was reported *(3)* that at 200 °C roughly half of the O_2 consumed in the gasification processes goes to gaseous CO and CO_2, and about half chemisorbs strongly on the carbon surface as stable oxygen complexes. Surface coverage by these oxygen complexes increases with carbon burnoff and can reach nearly 100% at 75% burnoff *(7)*.

(ii) Carbon Gasification. The reactions for intermediate oxygenated complexes gasification can be schematized:

10.1021/es9812655 CCC: $19.00
Published on Web 12/02/1999

$$C(O) \rightarrow CO \quad (3a)$$

$$C(O) + {}^1/_2O_2 \rightarrow CO_2 \quad (3b)$$

$$C(O) + MeO \rightarrow CO_2 + Me \quad (4)$$

Equations 3a and 3b are the oxidative desorptions of surface complexes as gaseous products CO and CO_2; in eq 3b, oxygen sources can be different: for instance, C(O) + C(O) = CO_2 + C. Equation 4 represents the surface oxidation of carbon−oxygen complexes to gaseous CO_2 by the oxygen from a metallic site.

Eventually, depending on the temperature, some small aromatic compounds can be formed during the overall process; their subsequent reactions may lead to PCDD/PCDF formation *(6)*.

Results and Discussion

The empirical rate equation (eq 1 in ref *1*) postulates that the TOC loss as a function of time and temperature is the result of two simultaneous processes.

To represent the overall process, we use the following global reaction equations:

$$C + {}^1/_2O_2 \underset{k_{-1}}{\overset{k_1}{\rightleftharpoons}} C(O) \quad (5)$$

$$C + O_2 \xrightarrow{k_2} CO_2 \quad (6)$$

$$C(O) + {}^1/_2O_2 \xrightarrow{k_3} CO_2 \quad (7)$$

If reaction 5 is assumed to be the dissociative oxygen chemisorption, $k_{-1} = 0$. Either of eqs 5−7 can be an uncatalyzed or catalyzed step.

As uncatalyzed steps, eq 6 is the direct impingement of oxygen onto active carbon sites, whereas eqs 5 and 7 describe the activated oxygen dissociative chemisorption with intermediate surface oxygen complexes formation and their subsequent desorption as gaseous CO_2. CO formation (eq 3a) is not included because, in our experimental conditions, CO is eventually present in very low concentrations ($CO/CO_2 < 0.05$) (*1*).

In catalyzed steps, metal oxides, MeO, mediate the oxygen transfer to carbon. MeO may already be present or it may form according to eq 2a. Here, eq 5 becomes eq 2b, eq 7 becomes eq 4, and eq 6 can be, for instance, a global reaction such as

$$C + MeO \xrightarrow{\text{slow}} CO + Me \quad (8a)$$

$$CO + {}^1/_2O_2 \xrightarrow{\text{fast}} CO_2 \quad (8b)$$

According to the proposed reaction scheme, the rate equations for C and C(O) are expressed by eqs 9 and 10.

$$d[C]/dt = -k_1^0\,[C][O_2]^{n1} - k_2^0\,[C][O_2]^{n2} \quad (9)$$

$$d[C(O)]/dt = k_1^0\,[C][O_2]^{n1} - k_3^0\,[C(O)][O_2]^{n3} \quad (10)$$

Following the experimental results in ref *1*, the oxidation reaction rates are assumed to be first order to native carbon C or C(O); moreover, as the ratio between oxygen and carbon concentrations is at least equal to 20, the oxygen terms in eqs 9 and 10 are assumed to be constants. We are currently studying the effects of both initial carbon concentration and reduced oxygen partial pressure. Equations 9 and 10 can be rewritten as eqs 9a and 10a

$$d[C]/dt = -(k_1 + k_2)[C] \quad (9a)$$

$$d[C(O)]/dt = k_1[C] - k_3[C(O)] \quad (10a)$$

where $k_i = k_i^0[O_2]^{ni}$.

The system of differential eqs 9a and 10a is solved analytically with the boundary condition [C(O)] = 0 at t = 0: $[C]_0$, i.e. [C] at $t = 0$, is equal to TOC^0. Thus the TOC decrease with time is given by eq 11:

$$\frac{TOC}{TOC^0} = \frac{[C] + [C(O)]}{[C]_0} = \frac{k_1}{(k_1 + k_2 - k_3)}\exp(-k_3 t) + \frac{(k_2 - k_3)}{(k_1 + k_2 - k_3)}\exp[-(k_1 + k_2)t] \quad (11)$$

The model contains three parameters k_1, k_2, and k_3. As for the empirical rate law, eq 1 in ref *1*, eq 11 is the sum of two exponentials, where the preexponential terms are combinations of kinetic constants, thus explaining the dependence of C_i and C_j on temperature.

The experimental TOC-time data for fly ash reactions (Supporting Information in ref *1*) were fitted to eq 11 using a nonlinear estimation procedure *(1)*. The goodness of fits as well as the statistical differences between two activation or thermodynamic parameters were estimated using the procedures reported in the same reference.

Tables 1−4 show the calculated values of the rate constants, k_1, k_2, and k_3 together with the determination coefficient, R^2. The activation and thermodynamic parameters calculated using Arrhenius and Eyring equations are reported in Tables 5 and 6.

To reinforce the very good agreement between the experimental data and the kinetic model, some data for FA2b are graphically reported as an example: Figure 1 shows the experimental and the calculated dependence on time of the C and C(O) concentrations as well as of their sum, all expressed as TOC, at two selected temperatures. The time and temperature dependence of the C(O) intermediate concentrations are collected in Figure 2.

Figures 1 and 2 furnish very interesting qualitative information. First, it can be seen (Figure 1) that the direct CO_2 formation, eq 6, requires 3−6 h, depending on temperature. Second, the formation of intermediate complexes, eq 5, is practically complete in about 8 h at 250 °C, whereas (Figure 2) about 3 h are needed to reach the maximum of the C(O)-t curve; moreover, the latter time is quite independent, while the complexes concentration is strongly dependent on temperature. At the highest times and the lowest temperatures the residual TOC content is entirely due to the complex concentration; surface coverage by oxygen complexes reaches 100% of the residual carbon at about 2% burnoff. At the highest temperatures the residual TOC is the result of the balance between C(O) formation and oxidation. Finally, it can be observed (Figure 2) that the oxidation of the complexes is almost completed in 24 h at 600 °C. The main conclusion is that the intermediate C(O) oxidation is the rate-determining step of the overall process.

The native carbon reactivity can be interpreted by separating the contribution of the weight of the carbon involved in the oxygen complex formation, $w_{C(O)}$, from that involved in the direct oxidation, w_{CO2}. At each temperature, $w_{C(O)}$ can be calculated as the maximum value in each of the [C(O)]-t curves (Figure 2) if it is assumed that it is not affected by the consecutive oxidation reaction; of course, this approximation is better at the lower temperatures. By sub-

TABLE 1. FA1 Calculated Rate Constants k_1, k_2, and k_3 at Different Temperatures

T (°C)	$k_1 \pm \sigma$ (min^{-1})	$k_2 \pm \sigma$ (min^{-1})	$k_3 \pm \sigma$ (min^{-1})	R^2
225	$(8 \pm 6)\ 10^{-3}$	$(1.4 \pm 0.5)\ 10^{-3}$	$(1.0 \pm 0.5)\ 10^{-4}$	0.990
275	$(1.3 \pm 0.3)\ 10^{-2}$	$(2.9 \pm 0.5)\ 10^{-3}$	$(4.5 \pm 0.4)\ 10^{-4}$	0.991
375	$(4.8 \pm 0.5)\ 10^{-3}$	$(1.38 \pm 0.05)\ 10^{-2}$	$(7 \pm 1)\ 10^{-4}$	0.998
400	$(3 \pm 2)\ 10^{-3}$	$(2.0 \pm 0.1)\ 10^{-2}$	$(3 \pm 2)\ 10^{-3}$	0.997
500	$(2.6 \pm 0.8)\ 10^{-3}$	$(2.4 \pm 0.1)\ 10^{-2}$	$(2 \pm 1)\ 10^{-3}$	0.998
600	$(3.7 \pm 1.4)\ 10^{-3}$	$(2.8 \pm 0.2)\ 10^{-2}$	$(3 \pm 1)\ 10^{-3}$	0.997

TABLE 2. FA2a Calculated Rate Constants k_1, k_2, and k_3 at Different Temperatures

T (°C)	$k_1 \pm \sigma$ (min^{-1})	$k_2 \pm \sigma$ (min^{-1})	$k_3 \pm \sigma$ (min^{-1})	R^2
200	$(1 \pm 1)\ 10^{-2}$	$(3 \pm 3)\ 10^{-4}$	$(5 \pm 3)\ 10^{-5}$	0.678
250	$(5 \pm 5)\ 10^{-3}$	$(1.1 \pm 0.5)\ 10^{-3}$	$(1.1 \pm 0.8)\ 10^{-4}$	0.953
275	$(7 \pm 3)\ 10^{-3}$	$(2.6 \pm 0.7)\ 10^{-3}$	$(3.2 \pm 0.6)\ 10^{-4}$	0.991
325	$(6 \pm 2)\ 10^{-3}$	$(9 \pm 1)\ 10^{-3}$	$(4 \pm 1)\ 10^{-4}$	0.988
350	$(1.1 \pm 0.3)\ 10^{-2}$	$(1.6 \pm 0.3)\ 10^{-2}$	$(4 \pm 1)\ 10^{-4}$	0.982
400	$(1.9 \pm 0.7)\ 10^{-2}$	$(3.4 \pm 0.7)\ 10^{-2}$	$(7 \pm 3)\ 10^{-4}$	0.972
450	$(2.4 \pm 0.8)\ 10^{-2}$	$(7 \pm 1)\ 10^{-2}$	$(4 \pm 2)\ 10^{-4}$	0.972
475	$(3.9 \pm 0.6)\ 10^{-2}$	$(1.2 \pm 0.1)\ 10^{-1}$	$(3 \pm 1)\ 10^{-4}$	0.991
550	$(6.0 \pm 0.8)\ 10^{-2}$	$(2.5 \pm 0.2)\ 10^{-1}$	$(2 \pm 1)\ 10^{-3}$	0.998
600	$(2 \pm 1)\ 10^{-1}$	$(7 \pm 4)\ 10^{-1}$	$(1.1 \pm 0.2)\ 10^{-2}$	0.999

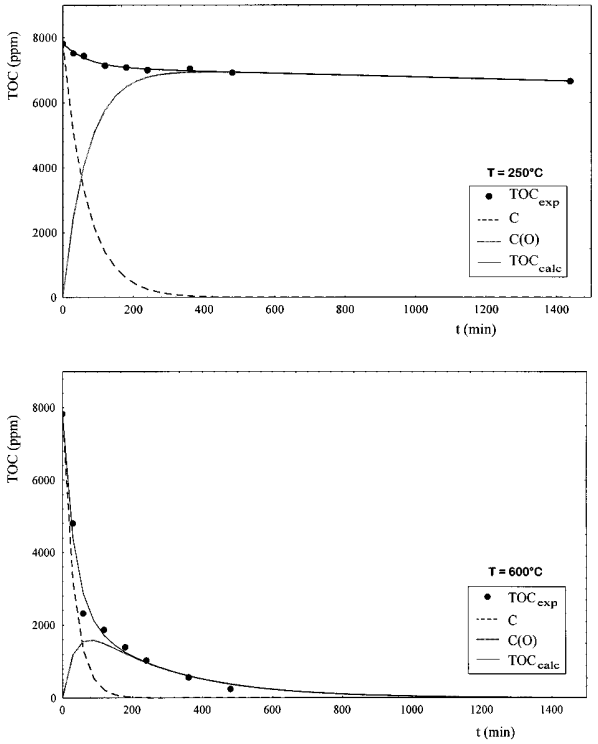

FIGURE 1. Experimental and calculated TOC along with the dependence on time of C and C(O) concentrations at 250 and 600 °C for FA2b.

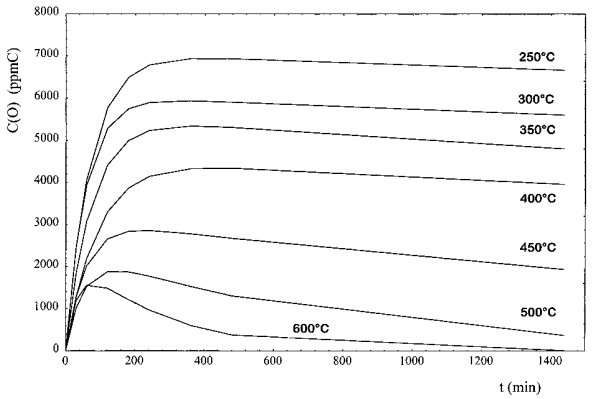

FIGURE 2. Time and temperature dependence of C(O) concentrations for FA2b.

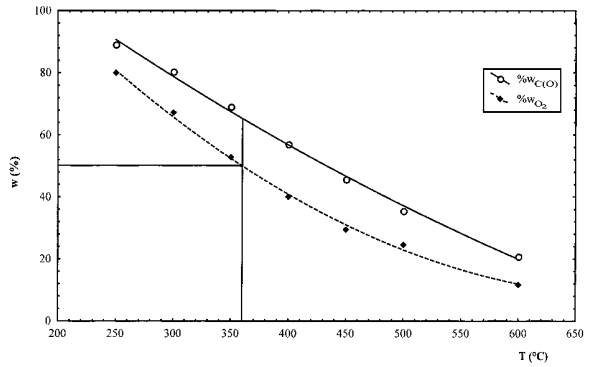

FIGURE 3. Intermediate oxygen complexes formation during native garbon gasification of FA2b: dependence on temperature of the weight of carbon (%$w_{C(O)}$, solid line) and the oxygen consumed (%w_{O2}, dotted line).

tracting these values from TOC^0, the corresponding weights w_{CO2} are obtained. Since the activation energy for carbon direct oxidation, Ea_2, is higher than that for oxygen chemisorption, Ea_1, the importance of carbon gasification to the overall interaction of O_2 with native carbon will increase with increasing reaction temperature. This is shown for FA2b in Figure 3, as a plot of $\%w_{C(O)}$ (solid line). Now, it is possible to estimate the percentage of the overall amount of O_2 consumed in the C(O) formation (dotted line in Figure 3): at 360 °C, roughly half of the O_2 consumed in the gasification process chemisorbs strongly on the carbon surfaces as stable oxygen complexes ($\%w_{C(O)} = 66$).

Fly ash reactivity can be evaluated by comparing the calculated rate constants both on the same fly ash and on different fly ashes. As also seen in Figure 4, where the Arrhenius plots for FA3 are reported, the k_2/k_1 ratios, i.e., the native carbon reactivity in the direct oxidation reaction (eq 6) and in the oxygen complexes formation (eq 5) increase with increasing temperature: the ratios are smaller than 1 at the lower temperatures, the inversion temperature being

TABLE 3. FA2b Calculated Rate Constants k_1, k_2, and k_3 at Different Temperatures

T (°C)	$k_1 \pm \sigma$ (min^{-1})	$k_2 \pm \sigma$ (min^{-1})	$k_3 \pm \sigma$ (min^{-1})	R^2
350	$(1.0 \pm 0.2)\ 10^{-2}$	$(3.9 \pm 0.4)\ 10^{-3}$	$(1.1 \pm 0.2)\ 10^{-4}$	0.994
400	$(6.4 \pm 0.7)\ 10^{-3}$	$(4.6 \pm 0.3)\ 10^{-3}$	$(1.0 \pm 0.2)\ 10^{-4}$	0.997
450	$(7 \pm 1)\ 10^{-3}$	$(1.09 \pm 0.08)\ 10^{-2}$	$(3.4 \pm 0.8)\ 10^{-4}$	0.995
500	$(6 \pm 3)\ 10^{-3}$	$(1.4 \pm 0.2)\ 10^{-2}$	$(1.3 \pm 0.8)\ 10^{-3}$	0.978
600	$(8 \pm 5)\ 10^{-3}$	$(2.1 \pm 0.3)\ 10^{-2}$	$(4 \pm 2)\ 10^{-3}$	0.988

TABLE 4. FA3, FA30, and FA3E Calculated Rate Constants k, k_2, and k_3 at Different Temperatures

T (°C)	$k_1 \pm \sigma$ (min^{-1})	$k_2 \pm \sigma$ (min^{-1})	$k_3 \pm \sigma$ (min^{-1})	R^2
		FA3		
275	$(6 \pm 2)\ 10^{-3}$	$(4.3 \pm 0.7)\ 10^{-3}$	$(1.0 \pm 0.7)\ 10^{-4}$	0.986
300	$(6 \pm 1)\ 10^{-3}$	$(6.4 \pm 0.8)\ 10^{-3}$	$(1.2 \pm 0.7)\ 10^{-4}$	0.991
350	$(1.7 \pm 0.6)\ 10^{-2}$	$(2.7 \pm 0.6)\ 10^{-2}$	$(3 \pm 2)\ 10^{-4}$	0.950
400	$(2.7 \pm 0.6)\ 10^{-2}$	$(6.1 \pm 0.8)\ 10^{-2}$	$(5 \pm 2)\ 10^{-4}$	0.975
450	$(4 \pm 1)\ 10^{-2}$	$(1.6 \pm 0.2)\ 10^{-3}$	$(8 \pm 5)\ 10^{-4}$	0.978
550	$(3.0 \pm 0.6)\ 10^{-2}$	$(3.3 \pm 0.2)\ 10^{-1}$	$(6 \pm 2)\ 10^{-3}$	0.998
		FA30		
300	$(6 \pm 3)\ 10^{-3}$	$(4 \pm 1)\ 10^{-3}$	$(2 \pm 2)\ 10^{-4}$	0.931
400	$(4 \pm 1)\ 10^{-2}$	$(6 \pm 1)\ 10^{-2}$	$(5 \pm 2)\ 10^{-4}$	0.965
500	$(7 \pm 3)\ 10^{-2}$	$(2.0 \pm 0.5)\ 10^{-1}$	$(3 \pm 2)\ 10^{-3}$	0.973
		FA3E		
300	$(5 \pm 3)\ 10^{-3}$	$(3.2 \pm 0.9)\ 10^{-3}$	$(1 \pm 1)\ 10^{-4}$	0.966
350	$(3.0 \pm 0.7)\ 10^{-2}$	$(2.7 \pm 0.5)\ 10^{-2}$	$(3 \pm 1)\ 10^{-4}$	0.967
400	$(3.0 \pm 0.5)\ 10^{-2}$	$(5.6 \pm 0.6)\ 10^{-2}$	$(4 \pm 1)\ 10^{-4}$	0.982
450	$(5 \pm 1)\ 10^{-2}$	$(8 \pm 1)\ 10^{-2}$	$(1.1 \pm 0.4)\ 10^{-3}$	0.970
500	$(4.3 \pm 0.7)\ 10^{-2}$	$(2.0 \pm 0.1)\ 10^{-1}$	$(2.5 \pm 0.6)\ 10^{-3}$	0.994

in the range 300−350 °C with the exception of FA2b (T = 425 °C). The k_2/k_3 ratios, i.e., the relative reactivity of the two oxidation reactions (equations 6 and 7), are greater than 1 and increase with increasing temperature, changing from about 5 to 300; on the contrary, the ratio decreases from 650 to 6 for FA2b. The evolution of these two ratios with temperature clearly shows the increasing importance of eq 6 with temperature increase. Finally, the k_1/k_3 ratios, i.e., the reactivity of the consecutive C(O) formation and oxidation reactions, are greater than 1 and decrease with increasing temperature.

To compare the reactivities of different fly ashes, we chose FA2b as a reference. For each j, the ratios k_1(FAj)/k_1(FA2b) and k_2(FAj)/k_2(FA2b) increase with increasing temperature, the former changing from about 0.1 to 25 and the latter from 1 to 2000; for k_1, the inversion temperature is in the range 250−300 °C. The ratios k_3(FAj)/k_3(FA2b) change from about 1 to 8000 with increasing temperature. These comparisons show a global lower reactivity of FA2b, the effect being greater at the higher temperatures: we are doing further experiments to understand the nature of this behavior.

To support the reaction mechanism, we focus first on the C−SiO_2 model system kinetics *(2)*. Here, the carbon gasification is uncatalyzed and follows a first-order kinetics. The Arrhenius plot exhibits two curves of distinctly different slopes which suggests that the mechanism of the carbon−oxygen interaction below 375 °C is different from one above this temperature.

The adsorption of O_2 on carbon, eq 5, is very slow at low reaction temperatures *(5)*: thus, for the activated carbon gasification in the lower temperature range (LTR, 325−375 °C), it seems reasonable to assume $k_1 \ll k_2$. Following this approximation, eq 11 becomes

$$\frac{\mathrm{TOC}}{\mathrm{TOC}^0} = \exp(-k_2 t) \qquad (11a)$$

In the LTR, the reaction rate is controlled by the inherent chemical reactivity of the carbon and the dominant process is the direct impingement of O_2 onto vacant carbon active sites, leading to some immediate carbon gasification (eq 6). This process is characterized by a $\Delta G^{\ddagger}$ value (about 285 kJ mol^{-1} at 723 K) essentially determined by the $\Delta H^{\ddagger}$ of 250 kJ mol^{-1}; the contribution of $\Delta S^{\ddagger}$ is almost zero. Such activation enthalpy corresponds to that for Saran char gasification in the 450−550 °C range (zone I): the shift to lower temperatures is due to the different carbon origin (6).

The optimal range for the dissociative chemisorption of molecular oxygen on carbon surface, eq 5, is between 400 and 500 °C (6): thus, for the C−SiO_2 model system in the higher temperature range (HTR, 375−600 °C), it seems reasonable to introduce $k_1 \gg k_2$ in eq 11, obtaining

$$\frac{\mathrm{TOC}}{\mathrm{TOC}^0} = \exp(-k_3 t) \qquad (11b)$$

i.e., the rate determining step is the surface diffusion of adsorbed oxygen to oxidize oxygen complexes. In the HTR, the $\Delta G^{\ddagger}$ of 240 kJ mol^{-1} (at 723 K) is mainly determined (89%) by a large negative $\Delta S^{\ddagger}$ (−0.295 kJ mol^{-1} K^{-1}); the low $\Delta H^{\ddagger}$ (27 kJ mol^{-1}) is in the range of activation energies for chemisorption of O_2 on carbon (20−50 kJ mol^{-1}) (5).

In both cases, a first-order rate equation is obtained, according to experimental results (2); both thermodynamic and kinetics arguments indicate that the HTR process is under a diffusion control.

The reactivity of the carbon in the DF−BPh−C−SiO_2 mixtures (1) is in very good agreement with the HTR carbon reactivity in the C−SiO_2 system.

The analysis of the fly ash activation and thermodynamic parameters, calculated for each of eqs 5−7 (Tables 5 and 6), and their comparison with those for the model systems allow for gaining information about the reaction mechanism.

According to eq 11a, the LTR parameters for C−SiO_2 must be compared with those for k_2. For FA2a and FA3 (including FA30 and FA3E), $\Delta H_2^{\neq}$ [Subscripts 1, 2, and 3 indicate the properties linked to the rate constants k_1, k_2, and k_3, i.e., to reactions in eqs 5, 6, and 7] (60−65 kJ mol^{-1}) is significantly

TABLE 5. Activation (Arrhenius equation) Parameters for Elementary Reactions

	ln (A/min)			Ea (kJ mol^{-1})		
	k_1	k_2	k_3	k_1	k_2	k_3
			FA1			
	$-(7.7 \pm 0.8)$	1.1 ± 0.9	$-(1 \pm 1)$	$-(13 \pm 7)$	31 ± 5	31 ± 8
R^2	0.70	0.92	0.80			
			FA2a			
	1 ± 1	8.3 ± 0.3	$-(1 \pm 1)$	27 ± 6	65 ± 1	34 ± 7
R^2	0.74	1.00	0.76			
			FA2b			
	$-(5.3 \pm 0.9)$	0.8 ± 0.8	4 ± 2	$-(2 \pm 5)$	33 ± 5	73 ± 12
R^2	0.47	0.94	0.92			
			FA3E			
	2.6 ± 0.7	9.1 ± 0.5	0.4 ± 0.5	35 ± 4	66 ± 3	44 ± 3
R^2	0.95	0.99	0.98			
			FA30			
	4 ± 2	10 ± 1	2 ± 2	45 ± 9	71 ± 7	52 ± 9
R^2	0.96	0.99	0.97			
			FA3E			
	3 ± 2	9 ± 2	1 ± 1	39 ± 13	71 ± 10	50 ± 8
R^2	0.74	0.94	0.93			

TABLE 6. Thermodynamic (Eyring Equation) Parameters for Elementary Reactions

	$-\Delta S^{\neq}$ (kJ K^{-1} mol^{-1})			$\Delta H^{\neq}$ (kJ mol^{-1})			$\Delta G^{\neq}$ at 723 K (kJ mol^{-1})		
	k_1	k_2	k_3	k_1	k_2	k_3	k_1	k_2	k_3
				FA1					
	$-(0.358 \pm 0.007)$	0.285 ± 0.008	0.30 ± 0.01	$-(18 \pm 9)$	26 ± 5	26 ± 8	240 ± 9	232 ± 5	246 ± 8
%ΔS							*92.3*	*88.9*	*89.5*
R^2	0.83	0.87	0.73						
				FA2a					
	0.284 ± 0.009	0.225 ± 0.002	0.30 ± 0.01	22 ± 5	60 ± 1	29 ± 7	227 ± 6	222 ± 1	248 ± 7
%ΔS							*90.5*	*73.2*	*88.2*
R^2	0.66	0.99	0.70						
				FA2b					
	$-(0.339 \pm 0.007)$	0.288 ± 0.007	0.26 ± 0.08	$-(9 \pm 5)$	27 ± 5	67 ± 12	237 ± 5	236 ± 5	253 ± 12
%ΔS							*96.4*	*88.4*	*73.7*
R^2	0.50	0.92	0.91						
				FA3E					
	0.272 ± 0.006	0.218 ± 0.005	0.291 ± 0.004	30 ± 4	61 ± 3	39 ± 3	227 ± 4	219 ± 3	249 ± 3
%ΔS							*86.7*	*72.1*	*84.4*
R^2	0.93	0.99	0.98						
				FA30					
	0.26 ± 0.02	0.21 ± 0.01	0.28 ± 0.01	40 ± 10	65 ± 8	47 ± 9	225 ± 10	220 ± 8	247 ± 9
%ΔS							*82.3*	*70.3*	*81.0*
R^2	0.95	0.99	0.96						
				FA3E					
	0.27 ± 0.02	0.21 ± 0.02	0.28 ± 0.01	33 ± 13	65 ± 10	44 ± 8	226 ± 13	221 ± 10	248 ± 8
%ΔS							*85.4*	*70.3*	*82.2*
R^2	0.68	0.93	0.91						

higher, whereas $\Delta S_2^{\neq}$ (-0.2 kJ K^{-1} mol^{-1}) and $\Delta G_2^{\neq}$ (220 kJ mol^{-1}) are significantly lower than the corresponding values for FA1 and FA2b (respectively, 25 kJ mol^{-1}, $-$ 0.3 kJ K^{-1} mol^{-1}, and 235 kJ mol^{-1}); moreover, the $\Delta S_2^{\neq}$ contribution to $\Delta G_2^{\neq}$ are 70% for FA2a and FA3 and 90% for FA1 and FA2b. In any case, the native carbon behavior is completely different from that of activated carbon in the LTR. According to the transition state theory, it is expected that the activation free energy for a reaction becoming catalyzed decreases via energetic stabilization: $\Delta G_2^{\neq} = 220-235$ kJ mol^{-1} and $\Delta H_2^{\neq} = 25-65$ kJ mol^{-1} must be compared with the corresponding values for C$-$SiO$_2$ reaction (285 and 250 kJ mol^{-1}). Moreover, the more orderly transition state required by a catalyzed reaction leads to a more negative activation entropy (-0.2 or -0.3 kJ K^{-1} mol^{-1}) in comparison with the uncatalyzed reaction (about 0 kJ K^{-1} mol^{-1}). Thus, the direct native carbon gasification (eq 6) is a catalyzed reaction which, according to the proposed mechanism, can result, for instance, from eqs 8a and 8b.

According to eq 11b, the HTR parameters for C$-$SiO$_2$ must be compared with those for reactions 5 and 7. For FA1 and FA2b, the activation energy for the oxygen chemisorption (eq 5) is near zero or negative and small; on the contrary, an activation energy is required for FA2a and FA3. For these fly ashes, $\Delta S_1^{\neq}$ (about -0.28 kJ K^{-1}mol^{-1}), $\Delta H_1^{\neq}$ (about 30 kJ mol^{-1}), and $\Delta G_1^{\neq}$ (227 kJ mol^{-1}) are not significantly different, the $\Delta S_1^{\neq}$ contribution being about 90%.

The differences in fly ashes behavior may be explained remembering that fly ash surfaces are heterogeneous; moreover, the differences in the native carbon structures in

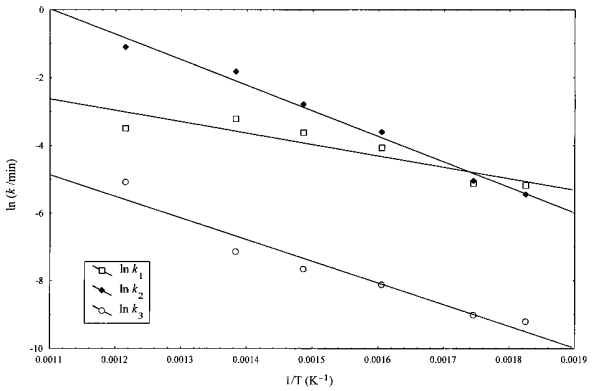

FIGURE 4. Arrhenius plots for FA3.

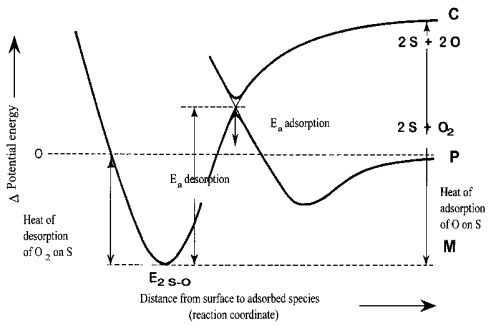

FIGURE 5. Diagram of the potential energy profile describing oxygen adsorption.

turn may lead to differences in the C(O) structure formed upon chemisorption. In fact, experimental evidence indicates that the heat of adsorption for different sites on the surface differs by 2 or more orders of magnitude (3). In terms of the classical potential energy surface describing chemisorption (8), activation energy depends on the height of the crossing point (Figure 5) between the P curve (potential energy curve of the physical adsorption of molecular oxygen) and the C curve (chemisorption of atomic oxygen on the fly ash surface). The height of the crossing point is determined by the form of the potential energy curves, that is by the overall surface properties. For instance, different sites have different values of energy levels P, C, and M as well as different steepness of the curve C. Eventually, the crossing point falls below the level of zero energy; in this case, the chemisorption of oxygen on active sites is a nonactivated process. Thus, the lower Ea_1 for FA1 and FA2b can be the result of either a catalyzed step or a more complex mechanism involving a number of elementary steps.

For the oxidation of C(O) intermediate complexes (eq 7), activation and thermodynamic parameters calculated from k_3 are not significantly different for all fly ashes except FA2b; the average $\Delta G_3^{\neq}$ value is 248 kJ mol^{-1}, with 85% $\Delta S^{\ddagger}$ contribution ($\Delta S_3^{\neq} = -0.29$ kJ K^{-1}mol^{-1} and $\Delta H_3^{\neq} = 37$ kJ mol^{-1}). These values are practically coincident with those for the HTR of C−SiO_2 system and the activated carbon in DF−BPh−C−SiO_2 mixture (240 and 242 kJ mol^{-1}; − 0.285 and − 0.29 kJ K^{-1} mol^{-1}; 27 and 35 kJ mol^{-1}, respectively). Moreover, the ratio of k_c (the rate constant for the C−SiO_2 in the HTR; ref 7) to k_i (the rate constant for carbon in the DF−BPh−C−SiO_2 system; ref 1) or k_3 are very similar (about 1.5 and 4.0, respectively). Thus, it seems reasonable to conclude that the chemical reaction expressed by eq 7 not only is the same both in model systems and fly ashes but occurs with the same uncatalyzed mechanism too.

In conclusion, the results of this study indicate that the measured conversion of native carbon in fly ashes to CO_2 is the result of two simultaneous processes taking place at the fly ash surface: the dissociative oxygen chemisorption followed by the uncatalyzed gasification of the intermediate complexes (eqs 5 and 7) and the oxygen transfer from a metal oxide site to a vacant carbon active site leading to a catalyzed carbon gasification. Due to the lowering of the $\Delta G_2^{\neq}$ value, the two reactions become concurrent on fly ash surface; thus the global mechanism on fly ash depends on interactions between native carbon and fly ash surface.

Acknowledgments

We thank Massimo Ferri for his valuable work in the laboratory, the "Fondazione Lombardia per l'Ambiente", and the Italian CNR (National Research Council) for financial support (Grant no. 97.03799.PS13).

Literature Cited

(1) Lasagni, M.; Collina, E.; Tettamanti, M.; Pitea, D. Environ. Sci. Technol. **2000**, 34, 130−136.
(2) Lasagni, M.; Collina, E.; Tettamanti, M.; Pitea, D. Environ. Sci. Technol. **1996**, 30, 1896−1901.
(3) Ismail, I. M. K.; Walker, Jr., P. L. Carbon **1989**, 27, 549−559.
(4) Milligan, M. S.; Altwicker, E. Environ. Sci. Technol. **1996**, 30, 230−236.
(5) Essenhigh, R. H. Fundamentals of Coal Combustion. In The Chemistry of Coal Utilization, 2nd Suppl.; Elliott, M. A., Ed.; Wiley: New York, 1981; pp 1153−1312.
(6) Huang, H.; Buekens A. Sci. Total. Environ. **1997**, 193, 121−141.
(7) Su, J. L.; Perlmutter D. D. AIChE J. **1985**, 31, 1725−1727.
(8) Thomas, J. M.; Thomas, W. J. Introduction to the Principles of Heterogeneous Catalysis; Academic Press: London, 1967; Chapter 2.

Received for review December 4, 1998. Revised manuscript received October 14, 1999. Accepted October 19, 1999.

ES9812655